



ACADÉMIE  
DES SCIENCES  
INSTITUT DE FRANCE

# *Comptes Rendus*

---

## *Géoscience*

### *Sciences de la Planète*


Félix Nenadji Djerosssem, Benoît Joseph Mbassa, Olivier Vanderhaeghe  
and Michel Gregoire

**The Iriba alkaline basalts, an expression of mantle-derived Cretaceous magmatism  
of the Cameroon-Chad volcanic line along the Central Africa Rift System**

Volume 356 (2024), p. 231-248

Online since: 20 December 2024

<https://doi.org/10.5802/crgeos.282>

 This article is licensed under the  
CREATIVE COMMONS ATTRIBUTION 4.0 INTERNATIONAL LICENSE.  
<http://creativecommons.org/licenses/by/4.0/>



*The Comptes Rendus. Géoscience — Sciences de la Planète are a member of the  
Mersenne Center for open scientific publishing*  
[www.centre-mersenne.org](http://www.centre-mersenne.org) — e-ISSN : 1778-7025



Research article

# The Iriba alkaline basalts, an expression of mantle-derived Cretaceous magmatism of the Cameroon-Chad volcanic line along the Central Africa Rift System

Félix Nenadji Djerosse<sup>Ⓜ,\*a</sup>, Benoît Joseph Mbassa<sup>Ⓜ,b</sup>, Olivier Vanderhaeghe<sup>Ⓜ,c</sup> and Michel Gregoire<sup>Ⓜ,c</sup>

<sup>a</sup> Institut National Supérieur du Sahara et du Sahel d'Iriba, Département des Mines, Energies Nouvelles et Renouvelables, Tchad

<sup>b</sup> Institute for Geological and Mining Research. P.O. Box 4110 Yaoundé, Cameroon

<sup>c</sup> GET-OMP, Université de Toulouse, UPS, CNRS, IRD, CNES, 14 avenue E. Belin, 31400 Toulouse, France

E-mail: [djerosse@gmail.com](mailto:djerosse@gmail.com) (F. Djerosse)

**Abstract.** The poorly documented volcanic rocks of the Ouaddai massif in Chad are a continuity of the ones of the Cameroon Volcanic Line further to the SE, located within the Central African rift system. New mineralogical and geochemical data from the Iriba basanites (SiO<sub>2</sub>: 41–45 wt%) show depletion in HREE, slight negative Sm anomaly and high LREE/HREE ratios, which is typical of OIB. The main differentiation process is fractional crystallization with a complete lack of crustal contamination. These features, similar to basanites exposed in southern Cameroon, reflect the partial melting of a metasomatized subcontinental lithospheric root reworked during the formation of the Cenozoic Central Africa Rift System. We propose to define by Cameroon-Chad Volcanic Line this continental scale structure controlling the emplacement of alkaline magmas.

**Keywords.** Chad volcanic activity, Iriba basanite, Fractional crystallization, HIMU-type mantle, Alkaline magmatism, Central Africa rift system.

**Funding.** LithoCOAC project (CNRS, France), IRN FALCoL (CNRS, France), French Embassy in Chad through the fellowship program “Séjour Scientifique de Haut Niveau (SSHN)”.

*Manuscript received 9 July 2024, revised 12 November 2024 and 25 November 2024, accepted 26 November 2024.*

## 1. Introduction

Alkaline magmatism, typical of intraplate environments including oceanic islands, continental rifts and intracontinental volcanoes, is generally the consequence of melting of peridotite in presence of CO<sub>2</sub> [Wyllie, 1977, Dasgupta et al., 2007, Baasner et al.,

2016], or of recycled oceanic crust [Green, 1973, Chase, 1981, Hofmann et al., 1986], or of metasomatized lithosphere [Halliday et al., 1995, Niu and O'Hara, 2003, Pilet et al., 2008]. Central Africa is made of the composite Archean to Palaeoproterozoic West Africa and Congo cratons bordered by Pan-African belts and Variscan orogenic belts [Figure 1; Bessoles and Trompette, 1980, Nzenti et al., 1988].

The published petrological data from the Cameroon Volcanic Line (CVL; Figure 1A) document

\* Corresponding author

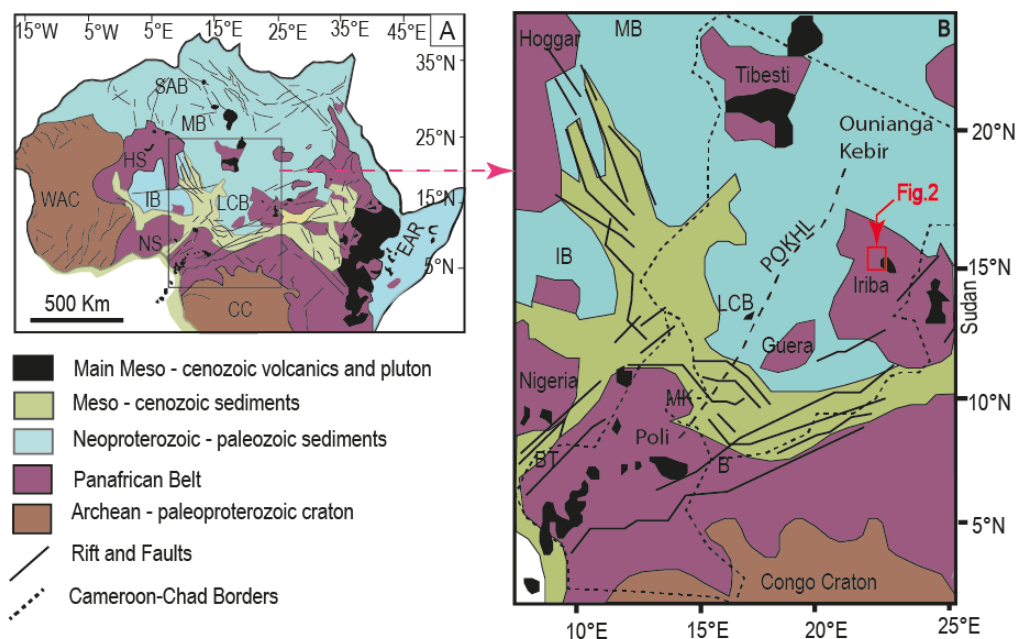


**Figure 1.** (A) Tectonic Map of Africa: Location map of the Cameroon Volcanic Line (CVL). The main geologic features of Africa are indicated. (B) Structural map of Central Africa Rift System [modified after Kogbe, 1981, Milesi et al., 2010] showing the Cameroon Volcanic Line (CVL) and its extension in chad. The names of the main Early Cretaceous intracontinental rifts are indicated. SAB = Sud Algerian Basin; MB = Murzuk Basin; IB = Iullemeden Basin; LCB = Lake Chad Basin; BT = Benue Trough; MK = Mayo Kebbi; B = Baïbokoum; WAC = West African Craton; CC = Congo Craton; HN = Hoggar Shield; NS = Nigerian Shield; EAR = East African Rift; POKH = Poli–Ounianga–Kebir heavy [Louis, 1970].

a typical bimodal series, marked by abundant mafic and felsic lavas and relatively sporadic occurrence in intermediate terms such as mugearites and benmoreites [Marzoli et al., 1999, 2000]. In contrast to this general trend, volcanoes at Bioko Island and Mount Cameroon are solely made of basaltic lavas, and a few massifs such as Manengouba or Bamenda-Bambouto Mountains display a complete range from mafic to felsic rocks [Kagou Dongmo et al., 2001, Kamgang et al., 2007, 2008]. Mafic lavas composition comprises basanites, basalts, and hawaiites while felsic lavas include trachytes, rhyolites and/or phonolites in a given volcanic massif. According to the available geochronological data, the oldest volcanic activity in the CVL (73 to 40 Ma) corresponds to anorogenic complexes, while the youngest ( $0.48 \pm 0.01$  Ma to present) are well expressed in volcanic massifs along the ocean-continent boundary and in the oceanic sector [Marzoli et al., 2000, Kagou Dongmo et al., 2010]. The parental magmas

generally display OIB features consistent with mantle plume activity, and originate from partial melting of various primitive mantle sources influenced by components such as HIMU or FOZO [Fitton, 1987, Halliday et al., 1990, Mbassa et al., 2012].

The CVL is marked by a NE–SW trending positive gravity anomaly in the continuity of the "Poli–Ounianga–Kebir heavy line" extending from Cameroon to Chad [Figure 1B; Louis, 1970]. This gravity anomaly marks the northern border of the Adamawa plateau [Poudjom Djomani et al., 1992, 1997]. The crustal structure beneath the Cameroon Volcanic line is marked by a 10 km thick crust that contrasts with the 40 km thick crust along its edges [Poudjom Djomani et al., 1997, Tokam Kamga et al., 2010, Eloumala et al., 2014]. The mantle transitional zone beneath the CVL is approximately located at  $250 \pm 10$  km [Reusch et al., 2010].

The West and Central African Rift System (WCARS), extending from the Hoggar to Cameroon

and Chad, is defined as a complex set of interconnected pull-apart, wrench and extension basins [Fairhead et al., 2013], associated with two magmatic series, of Mesozoic and Cenozoic age, respectively [Ye et al., 2017]. It is further delineated by Meso-Cenozoic sedimentary deposits along the margins of intracratonic basins (southern Algeria, Murzug, Iullemeden and Lake Chad basins), either on Neoproterozoic and Palaeozoic sequences or directly on the Pan-African basement [Ye et al., 2017; Figure 1A,B].

In this paper, we present mineralogical and whole rock geochemical data of the unstudied Iriba basanites in order to constrain their petrogenesis and discuss their link with the CVL and the Central Africa Rift.

## 2. Geological context of the west and central Africa rift system

According to the detailed work of Genik [1993], Guiraud and Maurin [1992], Mchargue et al. [1992], Fairhead et al. [2013], the evolution of the WCARS can be summarized as three stages: (1) Early Cretaceous opening of the rift marked by half basins in northern Nigeria and western Sudan with an E–W extension direction and opening of the Benue trough in Cameroon and Sudan with a NE–SW direction of extension, (2) Mid-Cretaceous sag basin marked by deposition of sediments unconformably over the rift series, (3) Late Cretaceous to present-day rift inversion marked by upright folds, reverse and strike-slip faults and deposition of terrigenous sediments.

The Central Africa Rift System is parallel to the LVC in Cameroon and subdivides in (i) a northern branch delineated by the Lake Chad Basin and continuing towards the Tibesti massif, and (ii) an eastern branch delineated by sedimentary deposits south of the Guera massif and continuing towards the Iriba region in the Ouaddaï massif (Figure 1B).

### 2.1. Geological context of the central Africa rift system in Chad

The geology of Chad consists of a Precambrian basement covered by Mesozoic to Cenozoic sedimentary sequences deposited in the Iullemeden and Chad intracratonic basins and in the Benue and Léré rift basins that are also marked by the emplacement of

volcanic rocks [Figure 1B; Bessoles and Trompette, 1980, Guiraud and Maurin, 1992, Milesi et al., 2010]. The volcanic rocks of Lake Chad (Hadjer Lamis), emplaced in the Cretaceous–Paleocene transition, are composed mainly of peralkaline rhyolites produced by fractional crystallization of parent magmas corresponding to alkaline basaltic melts, originating from a metasomatized mantle source [Mbowou et al., 2012, Shellnutt et al., 2016]. Based on geochronological and isotopic data, Shellnutt et al. [2016] suggest that silicic volcanic rocks from Lake Chad region are related to Late Cretaceous extensional volcanism in the Termit Basin. They conclude that magmatism was structurally controlled by Pan-African suture zones that were reactivated during the opening of the central Atlantic Ocean.

The Tibesti Volcanic Province (TVP; Figure 1B) represents the main volcanic activity in Chad. It is made of a variety of magmatic series including (i) Miocene Plateau volcanism consisting of flood basalts and silicic lava, with intercalated ignimbritic sheets emplaced from 17 to 8 Ma; (ii) basaltic cinder cones and associated lava flows emplaced from 7 to 5 Ma; (iii) Late Miocene large central composite volcanoes located along a major NNE–SSW trending fault; (iv) Large ignimbritic volcanoes (7–0.43 Ma); and (v) the Tarso Toussidé Volcanic Complex. The volcanic rocks are localized along the southwestern NW–SE Tassilian flexure and an eastern NE–SW to NNE–SSW major fault zone [Deniel et al., 2015]. Geochemical data from Gourgaud and Vincent [2003] revealed the presence of alkaline volcanic rocks in Emi Koussi locality, forming a bimodal series made up of (1) a silica saturated suite, composed mainly of trachytes with a few trachyandesites and (2) a silica under-saturated suite, composed of basalts and phonolites. Overall, available geochemical and petrological data show that the volcanic activity is generally expressed by alkaline to peralkaline lavas ranging from basanites to arfvedsonite ± acmite-bearing rhyolites, all resulting from fractional crystallization of alkaline melts, probably originated from a metasomatized mantle source [Vicat et al., 2002, Gourgaud and Vincent, 2003].

In the northern part of Ouaddaï massif, theralites and basalts are exposed [Gsell and Sonnet, 1962]. The Iriba basalts (Figure 2) outcrop in dome-shape or massive peak depressions from which emerge a series of superimposed flows of limited thickness (1 to

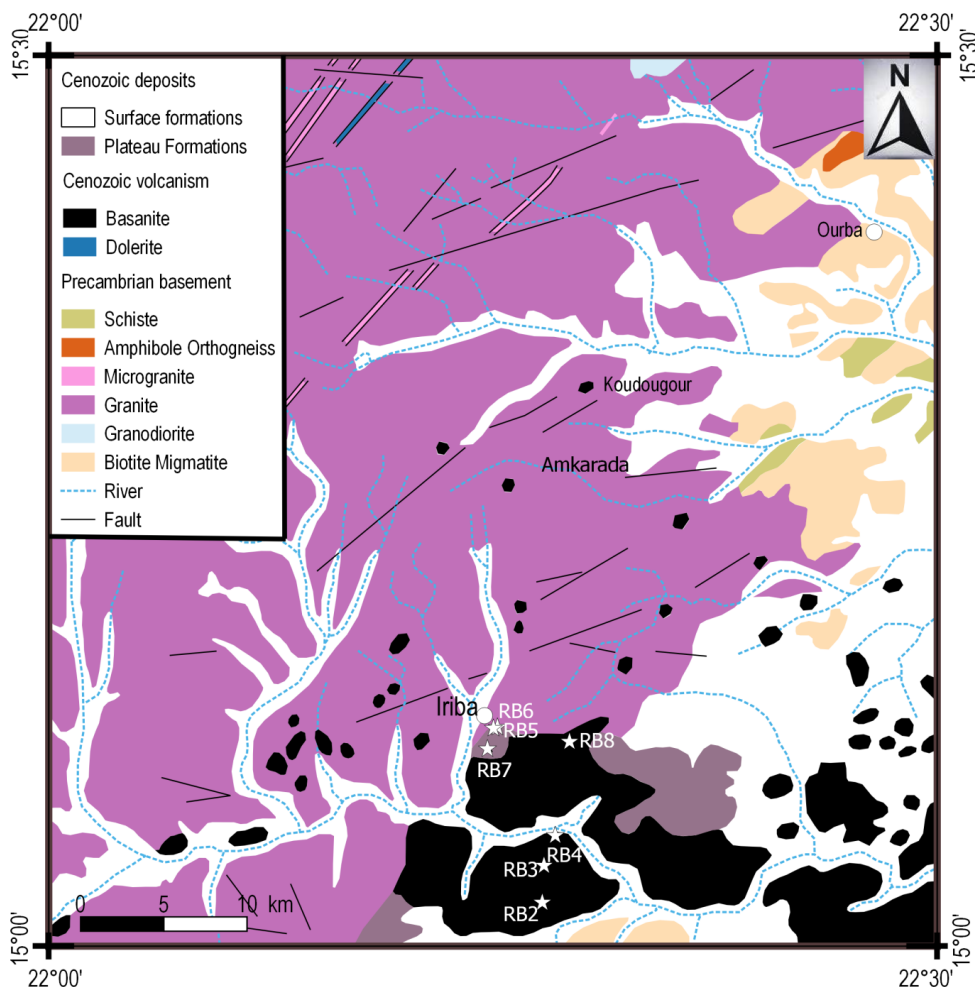


**Figure 2.** Geological map of Iriba and the surrounding area, extracted from the geological reconnaissance map of the Equatorial African States, Niéré sheet N° ND 34 NE 0.80-E.81 [Gsell and Sonnet, 1962].

2 m), laying on plateau formations resulting from the weathering of basement rocks, or Paleozoic sandstones [Gsell and Sonnet, 1962]. Seven (7) samples have been selected for petrological and geochemical study.

### 3. Analytical methods

Powders and thin sections of selected rock samples were prepared at the laboratory Geosciences Environment Toulouse, (GET-OMP-University of Toulouse 3, France) for geochemical and mineralogical analyses. Approximately 200 to 500 g of each sample was ground in a steel jaw crusher and then

pulverized in an agate ball mill. The powders were then digested using an alkaline fusion procedure where the powder was mixed with lithium metaborate and melted to produce a glass pellet. The pellet was digested in dilute nitric acid prior to analysis. Analyses and digestions were carried out at the Service d'Analyse des Roches et des Minéraux (SARM, CRPG, France); major elements were determined by ICP-OES while trace elements were determined by ICP-MS following the procedure described in Carignan et al. [2001].

The major elements minerals compositions were performed at the Centre de microcaractérisation Raimond Castaing (Toulouse, France), using a CAMECA

SX-Five Electron Probe Microanalyser. All analyzed samples were carbon coated (15 nm thick layer, density 2.25 g/cm<sup>3</sup>) before being introduced into the electron microprobe. The beam conditions were 15 kV accelerating voltage and 10 or 20 nA probe current. The synthetic and natural standards used for calibration were: albite (Na), corundum (Al), wollastonite (Si, Ca), sanidine (K), pyrophanite (Mn, Ti), hematite (Fe), periclase (Mg), Ni metal (Ni), Cr<sub>2</sub>O<sub>3</sub> (Cr) and reference zircon (Zr). Element and background counting times for most analyzed elements were 10 s or 5 s (for Na and K), whereas, peak counting times were 120 s for Cr and 80 to 100 s for Ni and 240 s for Zr. Detection limits were 70 ppm for Cr and Zr and 100 ppm for Ni.

#### 4. Petrography of the Iriba basanites

The Iriba basanites, are intrusive in the Paleozoic sandstones and are exposed as slabs or blocks within the plateau formations (Figure 3a,b). The Iriba basanites are characterized by a microlitic porphyritic texture (Figure 3c,d,f). Olivine, which constitutes 55 vol% of the rock, is present as sub-automorphic to xenomorphic phenocrysts and as microlites in the fine-grained groundmass. Olivine phenocrysts are fractured and altered into serpentine. Clinopyroxene represents 35 vol% of the rock and occurs as euhedral phenocrysts with clear cleavages and signs of corrosion. Plagioclase represents about 2–5 vol% and occurs as euhedral crystals with a dusty appearance due to the alteration. Opaque minerals (1–4 vol%) are sub-rounded or angular and generally included in olivine and clinopyroxene phenocrysts. Rare apatite (<2 vol%) is the only accessory mineral.

#### 5. Mineral chemistry

##### 5.1. Olivine

Olivine phenocrysts are magnesian (Fo<sub>69.52–90.28</sub> Fa<sub>09.72–39.48</sub>) with CaO ranging from 0.04 to 0.31 wt%. They are mostly chemically homogeneous but show slight chemical zoning with Fe enrichment from the core to the rim (Table 1). They are characterized by low MnO (0.05–0.31 wt%) and NiO (≤0.45 wt%) contents.

##### 5.2. Clinopyroxene

The selected pyroxenes analyses are reported in Table 2. Clinopyroxenes (Cpx) are Ca- and Mg- rich (Wo<sub>38.8–53.7</sub>–En<sub>33.4–43.2</sub>) with variable Fe composition (Fs<sub>12.4–23</sub>). According to the classification of Morimoto et al. [1988], the Cpx of Iriba basanites have a composition of diopside (Wo<sub>47.22–49.41</sub>En<sub>33.37–38.01</sub>Fs<sub>12.36–17.76</sub>) and augite (Wo<sub>38.75–43.07</sub>En<sub>38.23–43.22</sub>Fs<sub>13.71–23.02</sub>) (Figure 4). Some clinopyroxene crystals display Wo contents > 50%. Similar Cpx with Wo > 50% are commonly found in CVL such as basanites from Bamenda Mountains [Kamgang et al., 2008], Mbengwi [Mbassa et al., 2012] and Mount Bambouto [Wandji et al., 2000]. The phenocrysts are variably rich in Al<sub>2</sub>O<sub>3</sub> (2.96–9.94 wt%) and TiO<sub>2</sub> (0.4–4.49 wt%) with the highest contents of both Al and Ti in the crystals rims. Their Mg# vary from 66 to 88.

##### 5.3. Feldspars

Feldspar crystals are scarce in the studied basanites and correspond to Na-rich plagioclase (An<sub>2.09</sub>Ab<sub>80.10</sub>Or<sub>17.80</sub>) (Table 3).

##### 5.4. Opaque minerals

Opaque minerals (Table 3) are spinels (Mg<sub>3.58–60.08</sub>Fe<sub>39–99</sub>Mn<sub>0.18–0.80</sub>). They correspond to ulvospinel, magnetite and magnesioferrite according to the classification of Haggerty and Tompkins [1984] (Figure 5). The samples RB2 and RB7a are characterized by TiO<sub>2</sub> contents >0.20 wt% (0.95–15.81 wt%) with Fe<sup>2+</sup>/Fe<sup>3+</sup> ratios <2. These characteristics are indicative of their non-mantelic origin according to Kamenetsky et al. [2001]. They are also characterised by Cr# (100Cr/(Cr+Al)) ranging between 11.24 and 25.12 and are fairly NiO-rich (0.25–0.50 wt%) except RB3 which is NiO-poor (0.01 wt%).

#### 6. Whole rock geochemistry

##### 6.1. Major elements

Chemical analyses (major and trace elements) of Iriba lavas are reported in Table 4. SiO<sub>2</sub> contents range from 41 to 46 wt% and TiO<sub>2</sub> contents from 2.15 to 2.77 wt%, with high K<sub>2</sub>O+Na<sub>2</sub>O (4.97–6.59 wt%)

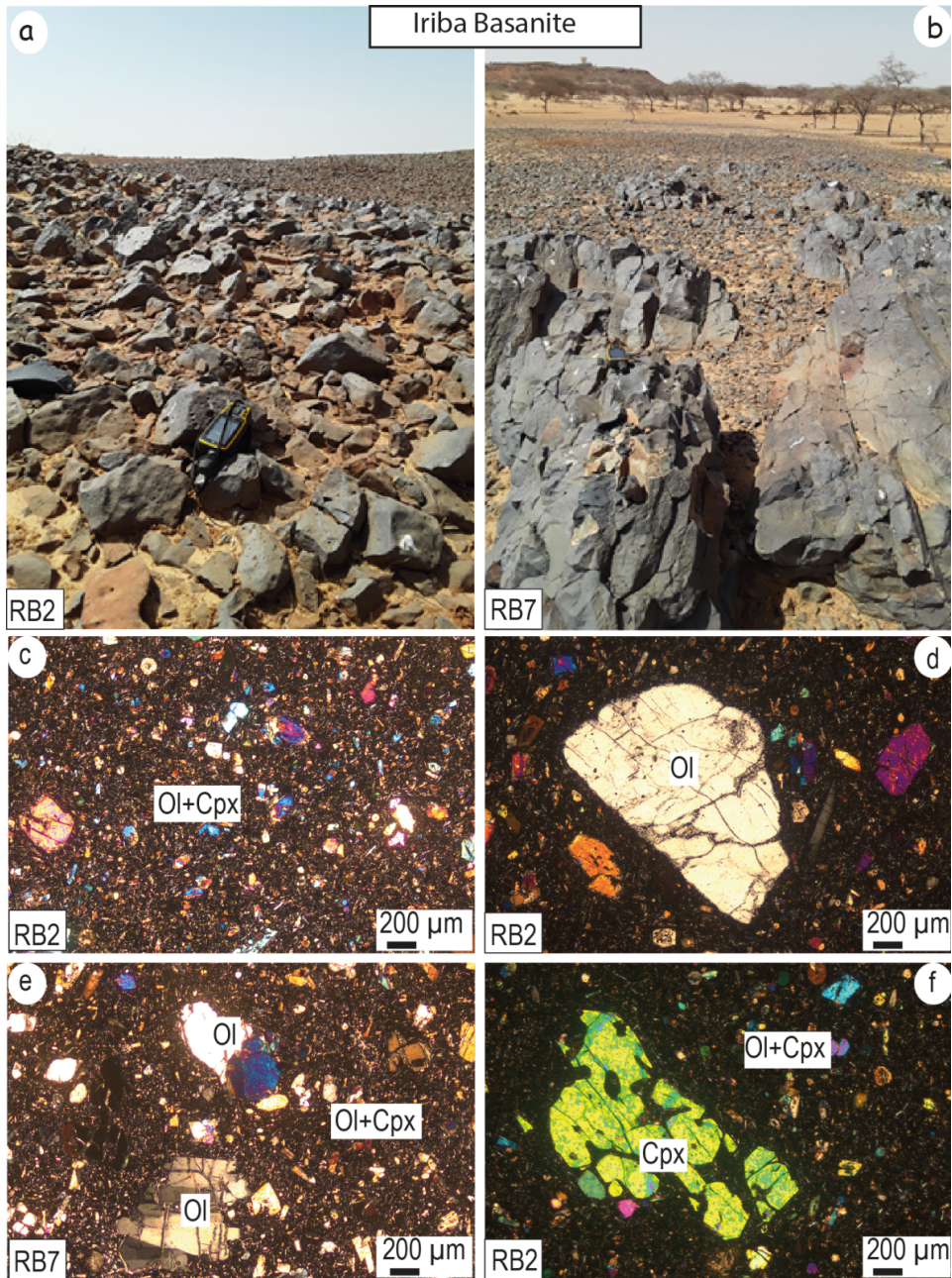


**Figure 3.** Different outcropping and representative photomicrographs of Iriba basanites. (a) Blocks; (b) slabs in the Paleozoic sandstone and plateau formations. (c) Porphyritic texture of basanites; (d) and (e) Olivine phenocrysts and microlitic groundmass; (f) corroded and resorbed clinopyroxene phenocryst and microlitic groundmass.

**Table 1.** Representative microprobe analyses of olivines from Iriba lavas

Sample	RB8	RB8	RB8	RB8	RB8	RB8	RB8	RB3	RB3	RB3	RB3	RB3	RB3
Analysis	C1	C2	C3	C4	C5	C5	C5	C1	C3	C4	C4	C5	C5
Position					r	c							
SiO <sub>2</sub>	39.71	40.24	40.01	39.69	40.33	39.80	38.72	40.17	40.32	38.90	39.37	40.97	39.59
TiO <sub>2</sub>	0.00	0.00	0.00	0.02	0.00	0.00	0.03	0.00	0.00	0.03	0.00	0.01	0.00
Al <sub>2</sub> O <sub>3</sub>	0.05	0.02	0.00	0.14	0.00	0.04	0.09	0.05	0.04	0.03	0.03	0.03	0.04
FeO	16.55	15.07	16.22	17.15	12.79	13.40	20.64	14.50	16.92	19.71	19.73	14.00	17.04
MnO	0.24	0.16	0.25	0.05	0.28	0.18	0.27	0.20	0.15	0.27	0.25	0.21	0.31
MgO	44.27	44.96	44.02	43.37	46.97	46.30	40.59	45.79	43.91	41.77	41.68	45.83	43.71
CaO	0.22	0.22	0.20	0.12	0.06	0.00	0.40	0.30	0.14	0.16	0.11	0.22	0.16
Total	101.04	100.67	100.70	100.54	100.43	99.72	100.74	101.01	101.48	100.87	101.17	101.27	100.85
Si	0.99	1.00	1.00	1.00	1.00	0.99	0.99	0.99	1.00	0.99	1.00	1.01	0.99
Ti	0.00	0.00	0.00	0.00	0.00	0.00	0.00	0.00	0.00	0.00	0.00	0.00	0.00
Al <sup>IV</sup>	0.00	0.00	0.00	0.00	0.00	0.00	0.00	0.00	0.00	0.00	0.00	0.00	0.00
Fe <sup>2+</sup>	0.35	0.31	0.34	0.36	0.26	0.28	0.44	0.30	0.35	0.42	0.42	0.29	0.36
Mn <sup>2+</sup>	0.01	0.00	0.01	0.00	0.01	0.00	0.01	0.00	0.00	0.01	0.01	0.00	0.01
Mg	1.65	1.67	1.64	1.63	1.73	1.72	1.55	1.69	1.63	1.58	1.57	1.68	1.64
Ca	0.01	0.01	0.01	0.00	0.00	0.00	0.01	0.01	0.00	0.00	0.00	0.01	0.00
Total	3.00	2.99	2.99	2.99	3.00	3.00	3.00	3.00	2.99	3.00	3.00	2.99	3.00
Fa	17.33	15.83	17.13	18.15	13.25	13.97	22.19	0.15	17.77	20.93	20.98	14.63	17.94
Fo	82.66	84.17	82.87	81.84	86.75	86.03	77.81	84.92	82.23	79.07	79.02	85.37	82.06
Sample:	RB2	RB2	RB2	RB2	RB2	RB7b	RB7b	RB7b	RB7b	RB7b	RB7b	RB7b	RB7b
Analysis:	C4	C4	C3	C3	C2	C2	C1	C1	C1	C2	C2	C2	C3
Position:	r				r			c			r		
SiO <sub>2</sub>	40.04	40.67	40.20	40.38	39.76	39.53	40.54	39.44	39.39	40.79	40.43	40.37	40.41
TiO <sub>2</sub>	0.00	0.02	0.00	0.00	0.00	0.01	0.01	0.02	0.00	0.00	0.00	0.02	0.01
Al <sub>2</sub> O <sub>3</sub>	0.03	0.02	0.12	0.03	0.05	0.08	0.06	0.03	0.03	0.09	0.04	0.06	0.04
FeO	12.33	12.38	15.49	15.79	18.77	15.13	14.46	19.59	19.64	14.71	14.24	14.93	14.25
MnO	0.19	0.17	0.21	0.22	0.31	0.24	0.25	0.20	0.30	0.21	0.25	0.23	0.19
MgO	47.97	47.95	44.68	44.65	42.25	45.51	46.02	42.15	41.98	45.94	46.35	45.57	46.63
CaO	0.18	0.10	0.24	0.23	0.25	0.21	0.22	0.12	0.11	0.19	0.30	0.30	0.28
Total	100.74	101.31	100.94	101.30	101.39	100.71	101.56	101.55	101.45	101.93	101.61	101.48	101.81
Si	0.98	0.99	1.00	1.00	1.00	0.99	1.00	0.99	0.99	1.00	0.99	1.00	0.99
Ti	0.00	0.00	0.00	0.00	0.00	0.00	0.00	0.00	0.00	0.00	0.00	0.00	0.00
Al <sup>IV</sup>	0.00	0.00	0.00	0.00	0.00	0.00	0.00	0.00	0.00	0.00	0.00	0.00	0.00
Fe <sup>2+</sup>	0.25	0.25	0.32	0.33	0.39	0.32	0.30	0.41	0.41	0.30	0.29	0.31	0.29
Mn <sup>2+</sup>	0.00	0.00	0.00	0.00	0.01	0.01	0.01	0.00	0.01	0.00	0.01	0.00	0.00

(continued on next page)



**Table 1.** (continued)

Sample	RB2	RB2	RB2	RB2	RB2	RB7b	RB7b	RB7b	RB7b	RB7b	RB7b	RB7b	RB7b
Analysis	C4	C4	C3	C3	C2	C2	C1	C1	C1	C2	C2	C2	C3
Position	r				r		c	c					r
Mg	1.76	1.75	1.66	1.65	1.58	1.69	1.69	1.58	1.58	1.68	1.70	1.68	1.71
Ca	0.00	0.00	0.01	0.01	0.01	0.01	0.01	0.00	0.00	0.00	0.01	0.01	0.01
Total	3.01	3.00	2.99	2.99	2.99	3.01	3.00	3.00	3.00	2.99	3.00	3.00	3.00
Fa	12.60	12.65	16.28	16.55	19.95	15.72	14.98	20.68	20.79	15.23	14.70	15.52	0.1463
Fo	87.40	87.35	83.72	83.45	80.05	84.28	85.01	79.32	79.21	84.77	85.30	84.47	85.37
Sample:	RB7b	RB7b	RB7b	RB7a	RB7a	RB7a	RB7a	RB7a	RB7a	RB7a	RB7a	RB7a	RB7a
Analysis	C3	C4	C4	C5	C5	C4	C4	C4	C3	C3	C1	C1	C1
Position:	r	r	c	r	c	r	c	m	r	c	r	c	r
SiO <sub>2</sub>	38.91	39.99	40.01	41.16	40.95	41.17	41.28	39.77	41.80	41.47	39.57	39.24	39.64
TiO <sub>2</sub>	0.00	0.00	0.00	0.00	0.01	0.00	0.00	0.03	0.00	0.00	0.02	0.00	0.02
Al <sub>2</sub> O <sub>3</sub>	0.04	0.06	0.02	0.03	0.04	0.06	0.06	0.06	0.04	0.03	0.05	0.07	0.07
FeO	21.59	14.64	14.71	9.56	12.29	12.97	12.28	15.93	9.80	9.75	20.15	18.43	19.67
MnO	0.26	0.19	0.20	0.13	0.20	0.17	0.18	0.24	0.14	0.15	0.22	0.27	0.25
MgO	40.65	46.61	45.88	49.84	47.67	46.57	47.46	44.29	49.23	49.35	41.42	42.89	42.06
CaO	0.17	0.16	0.10	0.06	0.21	0.18	0.18	0.31	0.09	0.09	0.27	0.29	0.23
Total	101.62	101.65	100.92	100.78	101.37	101.12	101.44	100.63	101.10	100.84	101.70	101.19	101.94
Si	0.99	0.99	0.99	1.00	1.00	1.01	1.00	1.00	1.01	1.00	1.00	0.99	1.00
Ti	0.00	0.00	0.00	0.00	0.00	0.00	0.00	0.00	0.00	0.00	0.00	0.00	0.00
Al <sup>IV</sup>	0.00	0.00	0.00	0.00	0.00	0.00	0.00	0.00	0.00	0.00	0.00	0.00	0.00
Fe <sup>2+</sup>	0.46	0.30	0.31	0.19	0.25	0.27	0.25	0.33	0.20	0.20	0.43	0.39	0.41
Mn <sup>2+</sup>	0.01	0.00	0.00	0.00	0.00	0.00	0.00	0.01	0.00	0.00	0.00	0.01	0.01
Mg	1.54	1.71	1.70	1.80	1.73	1.70	1.72	1.65	1.77	1.78	1.56	1.61	1.58
Ca	0.00	0.00	0.00	0.00	0.01	0.00	0.00	0.01	0.00	0.00	0.01	0.01	0.01
Total	3.01	3.01	3.00	2.99	2.99	2.98	2.98	3.00	2.98	2.99	3.00	3.01	3.00
Fa	22.95	14.98	15.24	9.71	12.63	13.51	12.67	16.79	10.04	9.98	21.44	19.42	20.78
Fo	77.04	85.02	84.76	90.28	87.36	86.49	87.32	83.21	89.95	90.02	78.56	80.58	79.22

C = core; r = rim; m = microlite; FeO = FeO total.

and MgO contents expressed by Mg# (100 Mg/[Mg + Fe]) ranging between 56 and 65. According to the TAS diagram [after Le Bas et al., 1986; Figure 6], they are classified as basanites. All the samples are alkaline with a sodic tendency according to criteria defined by Irvine and Baragar [1971] and Middlemost [1975]. In the major elements Harker diagrams (Figure 7a), Al<sub>2</sub>O<sub>3</sub> and K<sub>2</sub>O contents are positively correlated with SiO<sub>2</sub> while MgO, TiO<sub>2</sub>, CaO and P<sub>2</sub>O<sub>5</sub> display a negative correlation.

## 6.2. Trace elements

Compatible or slightly incompatible trace element concentrations are variable: Sc (17–24 ppm), V (175–245 ppm), Cr (46–60 ppm), Co (307–660 ppm), Ni (192–372 ppm), Cu (45–60 ppm) and Zn (105–189 ppm) (Table 4). In the trace elements *x*–*y* diagrams (Figure 7b), highly incompatible elements such as Nb, Zr, La and Ta show positive trends with each other, while compatible trace elements such as Ni,

**Table 2.** Representative microprobe analyses of clinopyroxenes from Iriba lavas

Sample	RB3	RB2	RB2	RB2	RB2	RB2	RB2	RB7a	RB7a
Analysis	C2	C3	C2	C2	C2	C2	C1	C2	C1
Positions	c			b					
SiO <sub>2</sub>	51.19	48.16	50.75	49.95	49.90	50.31	50.08	45.67	43.29
TiO <sub>2</sub>	1.17	2.08	0.47	0.70	0.64	0.66	0.68	3.31	4.49
Al <sub>2</sub> O <sub>3</sub>	2.96	6.89	3.91	5.19	4.94	4.88	4.88	8.13	9.94
FeO	8.40	7.29	13.44	10.48	10.85	10.08	10.17	7.26	7.31
MnO	0.17	0.17	0.42	0.22	0.24	0.22	0.23	0.14	0.03
MgO	15.16	12.65	12.92	11.28	11.62	11.42	11.51	11.97	11.05
CaO	21.02	22.88	18.22	22.98	22.21	22.82	22.77	24.32	24.44
Na <sub>2</sub> O	0.56	0.74	0.55	0.82	0.81	0.72	0.78	0.36	0.45
Total	100.63	100.86	100.68	101.62	101.21	101.11	101.10	101.16	101.00
Si	1.89	1.78	1.90	1.86	1.86	1.87	1.87	1.70	1.62
Ti	0.03	0.06	0.01	0.02	0.02	0.02	0.02	0.09	0.13
Al <sup>IV</sup>	0.11	0.22	0.10	0.14	0.14	0.13	0.13	0.30	0.38
Al <sup>VI</sup>	0.02	0.08	0.07	0.08	0.08	0.09	0.08	0.06	0.06
Fe <sup>3+</sup>	0.09	0.10	0.05	0.12	0.12	0.08	0.10	0.12	0.14
Fe <sup>2+</sup>	0.17	0.12	0.37	0.21	0.22	0.24	0.22	0.10	0.08
Mn <sup>2+</sup>	0.01	0.01	0.01	0.01	0.01	0.01	0.01	0.00	0.00
Mg	0.84	0.70	0.72	0.62	0.65	0.63	0.64	0.66	0.62
Ca	0.83	0.91	0.73	0.91	0.89	0.91	0.91	0.97	0.98
Na	0.04	0.05	0.04	0.06	0.06	0.05	0.06	0.03	0.03
Total	4.03	4.03	4.01	4.03	4.03	4.02	4.03	4.04	4.04
Wo	43.07	49.41	38.75	48.86	47.22	48.81	48.55	52.02	53.66
En	43.22	38.01	38.23	33.37	34.37	33.99	34.14	35.62	33.76
Fs	13.71	12.58	23.02	17.76	18.41	17.20	17.31	12.36	12.58

C = core; b = rim; FeO = FeO total.

Cr, Co and V show negative trends. REE element contents (Figure 8a) show enrichment in LREE ( $14.37 \leq (\text{La/Yd})_N \leq 24.82$ ) compared to MREE and HREE ( $2.73 \leq (\text{Gd/Yb})_N \leq 4.46$ ).

## 7. Discussion

### 7.1. Magmatic differentiation of the Iriba basanites

Given their low silica contents, their high Ni (207–372 ppm) and Cr (45–597 ppm) contents most of the Iriba basanites, might be considered as crystallized from a primary magma as defined by Frey et al.

[1978], even though they display a MgO content (8.6–12 wt%; Mg#  $\leq 65$ ) slightly below the one of the primary magmas. These characteristics may be consistent with an evolution through fractional crystallization with or without crustal contamination. The relative contributions of these processes can be deciphered from the analysis of major and trace elements compositions. The negative correlations of CaO concentration with SiO<sub>2</sub> and of Ni, Cr, Co and V with Th (Figure 8a,b), suggest fractionation linked to the crystallization of olivine, clinopyroxene, oxides and feldspar. Olivine and clinopyroxene fractionation are further suggested by the linear trend in the Sr versus Ba diagram [Franz et al., 1999, Figure 9b]. The positive correlations of Al<sub>2</sub>O<sub>3</sub> with SiO<sub>2</sub> and that of

**Table 3.** Representative microprobe analyses of feldspars and opaque minerals from Iriba lavas

Feldspars		Opaque minerals			
Sample	RB2-C3	Sample	RB3	RB2	RB7a
Analysis	C3	Analysis	C5	C2	C3
Position	r	Position			
SiO <sub>2</sub>	68.55	SiO <sub>2</sub>	0.77	0.00	0.14
Al <sub>2</sub> O <sub>3</sub>	19.71	TiO <sub>2</sub>	15.81	0.05	0.97
FeO	0.15	Al <sub>2</sub> O <sub>3</sub>	1.63	0.02	46.49
CaO	0.46	FeO	71.32	78.18	20.30
Na <sub>2</sub> O	9.74	Fe <sub>2</sub> O <sub>3</sub>	7.93	8.69	2.26
K <sub>2</sub> O	3.29	Cr <sub>2</sub> O <sub>3</sub>	0.32	0.01	12.24
Total	101.90	MnO	0.59	0.14	0.18
Si	11.91	MgO	1.50	0.00	17.29
Al	4.04	NiO	0.01	0.50	0.25
Fe total	0.02	Total	99.88	87.59	100.12
Ca	0.09	Ti	0.39	0.00	0.02
Na	3.28	Al	0.06	0.00	1.16
K	0.73	Fe <sup>2+</sup>	0.32	0.00	0.00
Total	20.07	Fe <sup>3+</sup>	1.64	1.96	0.36
Or	17.80	Mg	0.07	0.00	0.54
Ab	80.10	Total	2.48	1.96	2.08
An	2.09	xMg	3.58	0.00	60.08
		xFe	95.61	99.82	39.57
		xMn	0.80	0.18	0.35

*r* = rim.

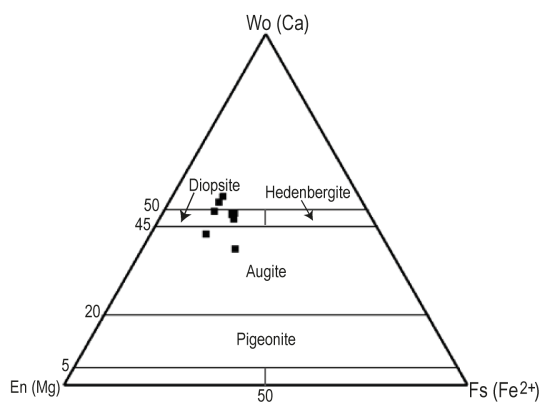


**Figure 4.** Ca-pyroxenes of Iriba basanites in Wo-En-Fs ternary diagram of Morimoto et al. [1988]. Wo = Wollastonite; En = Enstatite; Fs = ferrosilite.

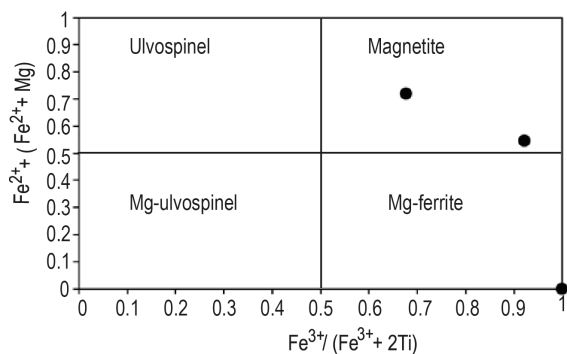


**Figure 5.** Composition of opaque minerals after Haggerty and Tompkins [1984].

Zr with Th likely imply a fractionation of plagioclase and zircon respectively. Fractional crystallization

**Table 4.** Whole rock composition of Iriba basanites

Sample	RB2	RB3	RB4	RB5	RB6	RB7	RB8
SiO <sub>2</sub>	45.53	43.50	42.38	44.73	42.66	41.60	44.29
Al <sub>2</sub> O <sub>3</sub>	13.91	13.15	13.09	13.69	13.14	12.91	13.54
Fe <sub>2</sub> O <sub>3</sub> t	12.58	12.92	13.84	12.63	13.98	13.39	14.23
MnO	0.21	0.20	0.25	0.18	0.23	0.19	0.20
MgO	8.86	10.41	9.38	10.15	9.01	12.27	8.92
CaO	9.57	11.31	10.58	9.85	10.67	11.27	10.34
Na <sub>2</sub> O	4.74	4.10	5.11	3.62	5.21	4.02	3.67
K <sub>2</sub> O	1.78	1.05	1.48	2.03	1.20	0.79	1.30
TiO <sub>2</sub>	2.15	2.70	2.67	2.51	2.77	2.72	2.55
P <sub>2</sub> O <sub>5</sub>	0.67	0.66	1.23	0.61	1.13	0.83	0.97
Total	100.00	100.00	100.01	100.00	100.00	99.99	100.01
Mg#	58.42	61.65	57.46	61.57	56.22	64.63	55.56
ppm							
Rb	36.92	25.88	24.18	42.39	67.47	50.01	50.87
Sr	969.28	742.93	1214.25	829.19	1189.9	887.15	985.83
Ba	592.63	476.46	665.51	446.71	627.85	597.08	510.53
V	175.43	244.85	203.58	211.12	201.81	236.67	181.67
Cu	58.23	60.31	45.12	57.50	45.22	56.24	53.44
Cr	48.63	57.48	45.92	53.86	50.72	59.68	54.30
Co	470.93	578.19	393.64	659.70	477.27	548.05	306.75
Ni	271.06	316.59	191.63	372.14	281.87	349.86	207.41
Sc	18.63	23.76	19.29	22.17	18.81	23.74	16.58
Zn	122.23	105.36	130.63	105.44	189.20	104.97	148.10
Y	25.41	20.28	31.83	21.46	30.58	25.42	22.96
Zr	227.56	194.78	374.16	214.35	328.14	164.37	241.31
Hf	4.72	4.37	7.52	4.65	6.73	3.95	5.19
Ta	3.30	3.42	6.66	3.37	5.93	3.09	3.64
Nb	50.96	49.53	94.20	47.24	84.81	44.96	53.44
La	40.07	34.26	69.95	33.21	67.28	39.93	48.51
Ce	79.29	67.99	134.75	66.12	130.58	81.20	96.50
Pr	9.19	8.01	15.29	7.79	14.85	9.71	11.15
Nd	36.30	32.07	58.65	31.32	57.17	39.25	44.43
Sm	7.59	6.73	11.15	6.62	11.05	8.33	9.15
Eu	2.50	2.16	3.46	2.15	3.45	2.68	2.92
Gd	6.61	5.65	9.03	5.76	9.05	7.11	7.57
Tb	0.98	0.81	1.26	0.83	1.25	1.01	1.04
Dy	5.44	4.44	6.84	4.57	6.76	5.56	5.36
Ho	1.01	0.81	1.26	0.85	1.22	1.02	0.92
Er	2.47	1.90	2.99	2.04	2.84	2.40	2.04
Tm	0.33	0.24	0.40	0.27	0.37	0.31	0.25
Yb	2.00	1.47	2.42	1.61	2.17	1.83	1.40
Lu	0.29	0.20	0.35	0.23	0.30	0.25	0.18
Th	4.98	4.09	8.73	4.27	8.15	3.36	5.06
U	1.32	1.17	2.71	1.21	2.28	0.95	1.36

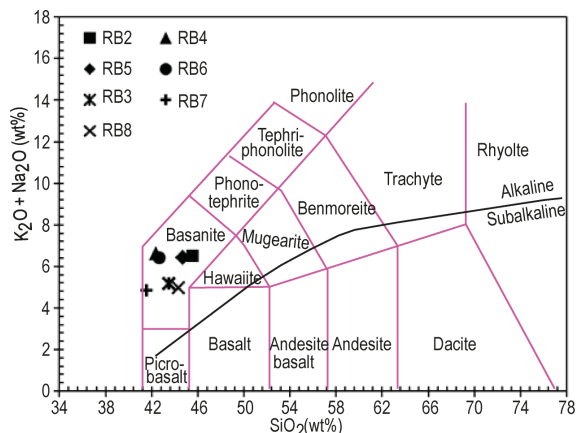


**Figure 6.** Total alkali-silica diagram [after Le Bas et al., 1986]. The dark line separates the alkaline and the subalkaline domain, according to Irvine and Baragar [1971].

is also consistent with (i) the enrichment in LREE, (ii) the similarity of hygromagmatophilic elements ratios such as Zr/Nb, Th/Hf and La/Ta, (iii) the parallelism of the REE patterns (Figure 8a,b), and (iv) the horizontal trend of the studied basanites in the Sr versus Rb diagram of Xu et al, 2007 (Figure 9a). Nevertheless, the relatively high Ni (192–350 ppm) and Co (307–660 ppm) contents of the basanites points to a low degree of fractional crystallization of the parental magma.

The range of  $P_2O_5$  contents of the studied basanites ( $0.6 < P_2O_5 < 1.9$ ) points to a complete lack of crustal contamination. This is confirmed in the  $K_2O/Th$  versus  $La/Ta$  diagram (Figure 10a,b), where the Iriba lavas fall within the field of uncontaminated basalts. Such features are similar to that of some lavas from northern Cameroon, notably the Ngaoundéré basaltic lavas [ $0.9 < P_2O_5 < 1.3$ ; Nkouandou et al., 2010]; [ $0.4 < P_2O_5 < 1.4$ ; Fitton, 1987] and the Kapsiki basalts [ $0.6 < P_2O_5 < 1.2$ ; Ngounouno et al., 2000].

### 7.2. Source of the Iriba basanites and conditions of partial melting

The Iriba basanites display characteristics of intraplate magmas (Figure 10a,b), generated by partial melting of an enriched mantle source. A similar intraplate signature is displayed by alkaline continental basalts exposed in Emi-Koussi in Chad [Gourgaud

and Vincent, 2003] and by alkaline basalts from Mayo Oulo-Léré, Babouri-Figuil, located at the Cameroon-Chad border Ngounouno et al. [2000]. The geochemical signatures of the Iriba basanites point to a higher degree of partial melting (2–4%) than the ones from Baossi-Warack [0.5–2%; Tiabou et al., 2018] and from Mt Cameroon [1–2%; Yokoyama et al., 2007] but lower than that of basanites from Mbengwi [5–8%; Mbassa et al., 2012].

Assuming that MREE/HREE ratios are sensitive to the amount of residual garnet in the source, the range of the studied Iriba basanites ( $Tb/Yb$ )<sub>N</sub> ratios (2.22–3.37) is higher than 1.7 and is consistent with the presence of garnet in the source, as proposed by Wang et al. [2002]. This interpretation is corroborated by the position of the Iriba basanites in the Gd/Yb versus La/Yb diagram (Figure 10c), which indicates partial melting of a lherzolitic mantle containing less than 8% of garnet, except for sample RB8, characterized by high levels of Gd and La but low levels of Yb. The ranges of some incompatible trace elements ratios such as Zr/Nb, La/Nb, Ba/Nb, Rb/Nb and Ba/La of Iriba basanites (Table 5) are typical of Ocean Island Basalts (OIB) defined by Zindler and Hart [1986]. This OIB affinity is also confirmed in the Nb/Y versus Zr/Y diagram of Weaver [1991], with an imposing role for recycled components and the HIMU-EM1 mantle poles, except one sample plotting close to the enriched EM2 pole (Figure 10d).

### 7.3. The Cameroon chad volcanic line

The Iriba basanites are similar to alkaline magmatic series emplaced along the Central Africa Rift System including in the north of the volcanic rocks of Lake Chad and the Tibesti Volcanic Province. The influence of Cretaceous–Paleocene to Cenozoic mantle-derived magmatism initially identified in Cameroon and the western part of Chad might thus be extended northeastward, up to the northern part of Ouaddaï massif, on both sides of the positive gravity anomaly of the “Poli–Ounianga–Kebir heavy line”. We proposed to defined this large SW–NE magmatic province as the Cameroon Chad Volcanic Line (CCVL). The Cretaceous–Paleocene to Cenozoic magmatic activity of the Cameroon-Chad Volcanic Line appears to be controlled by the opening of the Central Africa Rift System localized along the edges of Archean cratonic nuclei marked by tectonic

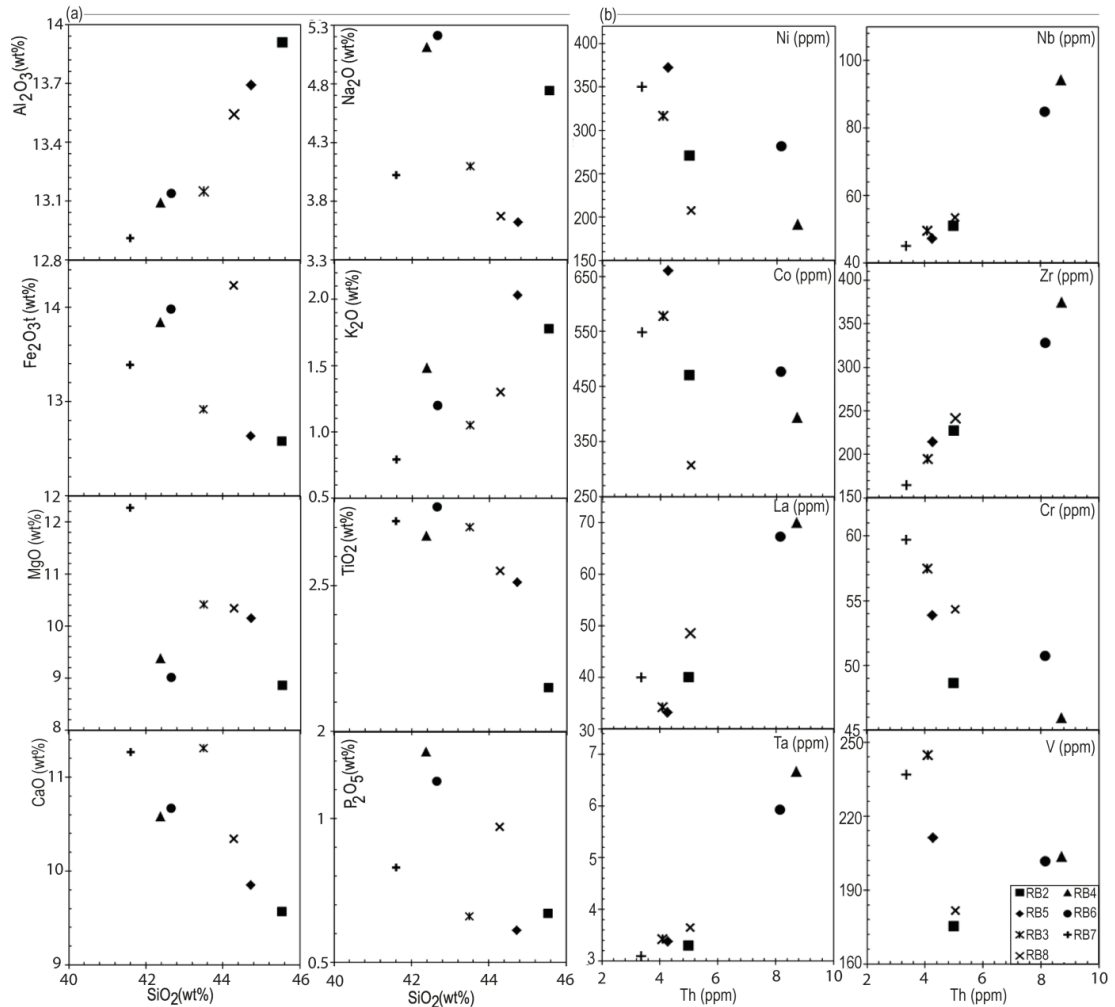


**Figure 7.** (a) Major elements (wt%) versus SiO<sub>2</sub> distribution; (b) Trace elements distribution (Th versus Ni, Nb, Co, Zr, La, Cr, Ta and V) of the Iriba basanites.

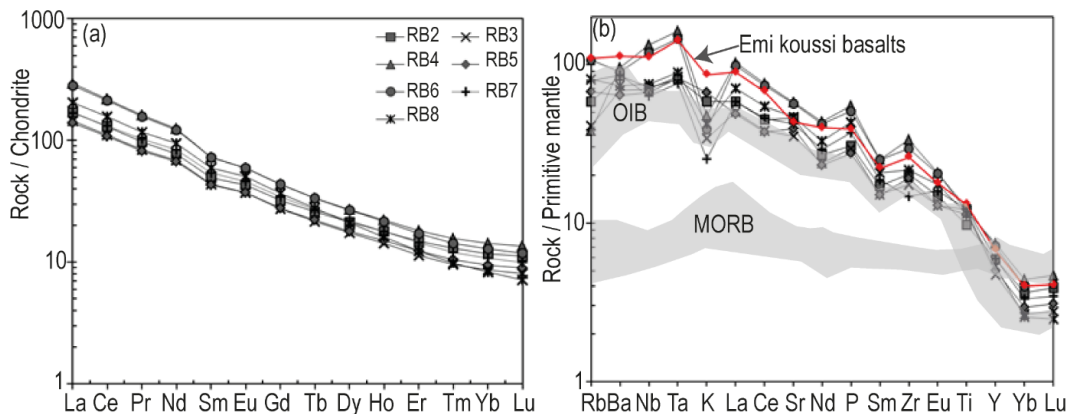


**Figure 8.** (a) Chondrite normalized REE patterns and (b) primitive mantle normalized trace elements diagrams of Iriba basanites. The normalization values are after Sun and McDonough [1989].

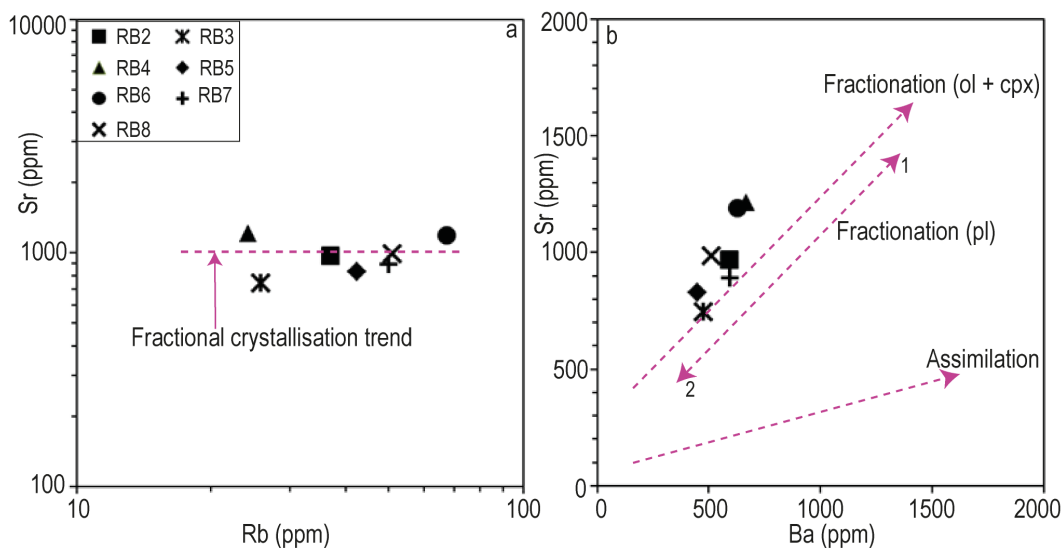


**Figure 9.** (a) Illustration of fractional crystallization trend in Rb versus Sr diagram [Xu et al., 2007] and (b) illustration of olivine and clinopyroxene fractionation in the Sr versus Ba diagram of Franz et al. [1999].

**Table 5.** Comparative incompatible elements contents of Iriba alkaline basanites with those of the crust and certain mantle reservoirs [Zindler and Hart, 1986]

	Zr/Nb	La/Nb	Ba/Nb	Rb/Nb	Ba/La
Iriba basanites	3.6–4.5	0.69–0.90	7.0–13.2	0.25–1.11	9.33–14.95
Continental crust	16.2	2.2	54	4.7	25
Primitive mantle	14.8	0.94	9	0.91	9.6
N-MORB	46.2	1.07	1.7–8.0	0.36	4
E-MORB	14.07	1.05	4.9–8.5	nd	nd
HIMU–OIB	3.2–5.6	0.66–0.77	4.9–6.9	0.35–0.38	6.8–8.7
EM1–OIB	4.2–11.5	0.86–1.19	11.4–17.8	0.88–1.77	13.2–16.9
EM2–OIB	4.5–7.3	0.89–1.11	7.3–13.3	0.59–0.85	8.3–11.3

reworking and accretion of juvenile Paleoproterozoic to Neoproterozoic crust.

## 8. Conclusion

In this contribution, we present the first petrographic, mineralogical and geochemical study of the Iriba basanites located in the northern part of the Ouaddaï massif. The Iriba basanites are composed of magnesian olivine, Ca-rich clinopyroxenes (diopside and augite), albite and spinel. They display sodic and alkaline affinities that are attributed to magmatic

differentiation of a primary mantle-derived magma by fractional crystallization. The geochemical signatures of these basanites indicate an affinity with OIB and are consistent with a generation by a low degree of partial melting (2–4%) of HIMU-type mantle source containing residual garnet (4–8%), without any crustal contamination. The Iriba basanites are similar to an alkaline magmatic series emplaced along the Central Africa Rift System, active from the Cretaceous–Paleocene to the Cenozoic, belonging to the so-called Cameroon Chad Volcanic Line (CCVL).

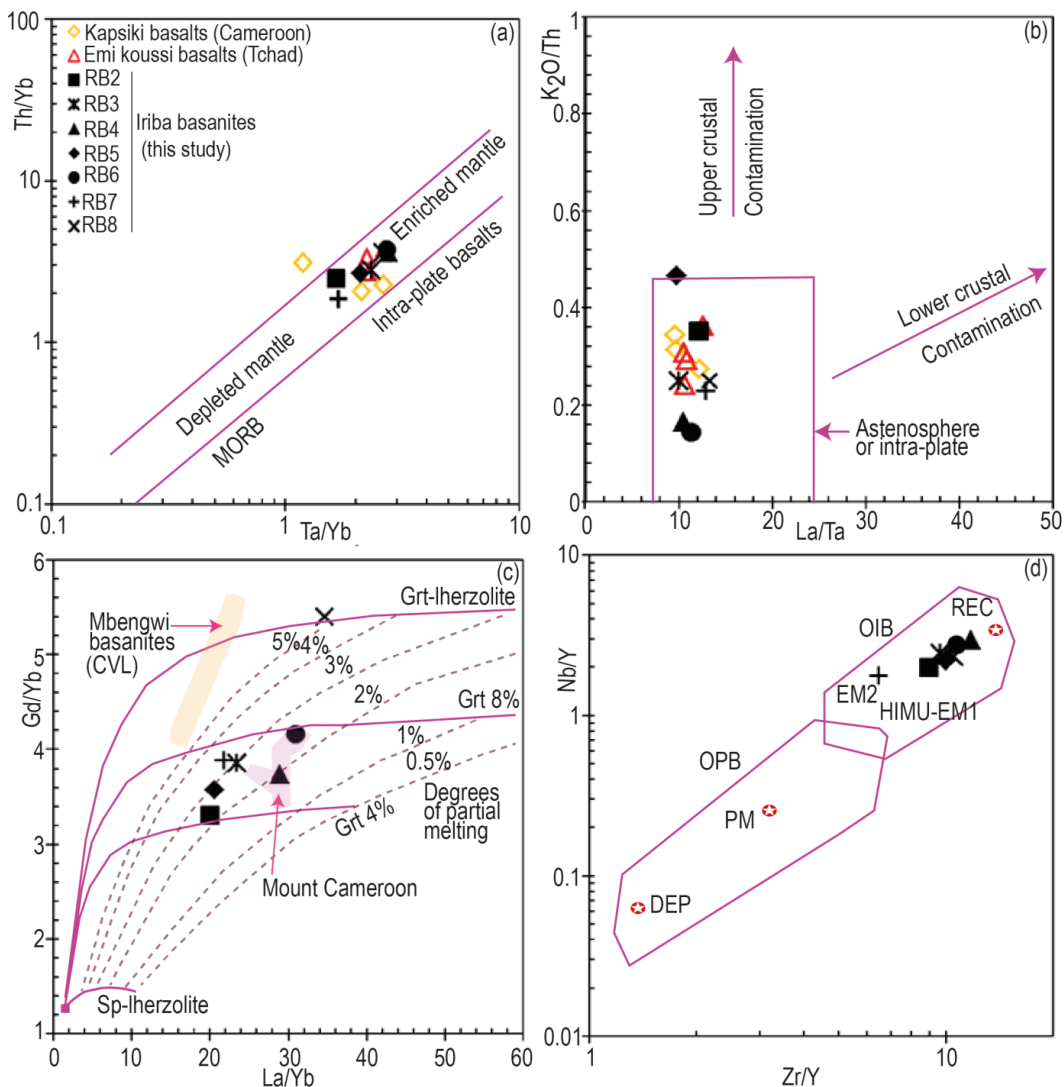


**Figure 10.** Position of the studied basanites in (a) Th/Yb versus Ta/Yb [from Pearce, 1982, 1983] and (b) K<sub>2</sub>O/Th versus La/Ta diagrams. (c) Gd/Yb versus La/Yb diagram [after Yokoyama et al., 2007] illustrating the partial melting of Iriba basanites. The curves at Grt 4% and 8% correspond to the garnet content in the source [Halliday et al., 1995]. CVL = Cameroon Volcanic Line. (d) Nb/Y versus Zr/Y diagram of Weaver [1991] and Condie [2005]. OIB = Ocean Island Basalts, OPB = Ocean Plateau Basalts, PM = primitive mantle, DEP = highly depleted mantle, REC = recycled component; HIMU = high <sup>238</sup>U/<sup>204</sup>Pb mantle source, EM1 and EM2 enriched mantle sources.

## Declaration of interests

The authors do not work for, advise, own shares in, or receive funds from any organization that could benefit from this article, and have declared no affiliations other than their research organizations.

## Funding

The research has been financially supported by LithoCOAC project (CNRS, France), the IRN FAL-CoL (CNRS, France) and the participation of the French Embassy in Chad through the fellowship



program “Séjour Scientifique de Haut Niveau (SSHN)”.

## Acknowledgements

We thank Philippe de Parseval for his assistance with electron microprobe analyses. Fabienne de Parseval is also thanked for the confection of rocks thin sections. We gratefully acknowledge several anonymous reviewers for their critical and constructive comments of the manuscript.

## References

- Baasner, A., Médard, E., Laporte, D., and Hoffer, G. (2016). Partial melting of garnet lherzolite with water and carbon dioxide at 3 GPa using a new melt extraction technique: implications for intraplate magmatism. *Contrib. Mineral. Pet.*, 171(5), 1–23.
- Bessoles, B. and Trompette, R. (1980). *La chaîne panafricaine. Zone mobile d'Afrique Centrale (partie sud) et zone soudanaise*, volume 92 of *Mémoire du Bureau de Recherches Géologiques et Minières*. Editions B.R.G.M., Orléans.
- Carignan, J., Hild, P., Mevelle, G., Morel, J., and Yeghicheyan, D. (2001). Routine analyses of trace elements in geological samples using flow injection and low pressure on-line liquid chromatography coupled to ICP-MS: A study of geochemical reference materials BR, DR-N, UB-N, AN-G and GH. *Geostand. Newslett.*, 25, 187–198.
- Chase, C. G. (1981). Oceanic island Pb: two-stage histories and mantle evolution. *Earth Planet. Lett.*, 52, 277–284.
- Condie, K. C. (2005). High field strength element ratios in Archean basalts: a window to evolving sources of mantle plume. *Lithos*, 79, 491–504.
- Dasgupta, R., Hirschmann, M. M., and Smith, N. D. (2007). Partial melting experiments of peridotite + CO<sub>2</sub> at 3 GPa and Genesis of Alkalic Ocean Island Basalts. *J. Pet.*, 48, 2093–2124.
- Deniel, C., Vincent, P. M., Beauvilain, V., and Gourgaud, A. (2015). The Cenozoic volcanic province of Tibesti (Sahara of Chad): major units, chronology, and structural features. *Bull. Volc.*, 77, article no. 74.
- Eloumala, O. P. N., Mouzong, P. M., and Ateba, B. (2014). Crustal structure and seismogenic zone of cameroon: integrated seismic, geological and geophysical data. *Open J. Earthq. Res.*, 3, 152–161.
- Fairhead, J. D., Green, C. M., Masterton, S. M., and Guiraud, R. (2013). The role that plate tectonics, inferred stress changes and stratigraphic unconformities have on the evolution of the West and Central African Rift System and the Atlantic continental margins. *Tectonophysics*, 594, 118–127.
- Fitton, J. G. (1987). The Cameroon Line, West Africa: a comparison between oceanic and continental volcanism. In Fitton, J. G. and Upton, B. G. J., editors, *Alkaline Igneous Rocks*, Geological Society, London, Special Publications, 30, pages 273–291. Geological Society of London.
- Franz, G., Steiner, G., Volker, F., Pudlo, D., and Hammerschmidt, K. (1999). Plume related alkaline magmatism in central Africa—the Meidob Hills (W Sudan). *Chem. Geol.*, 157, 27–47.
- Frey, F. A., Green, D. H., and Roy, S. D. (1978). Integrated models of basalts petrogenesis: a study of quartz tholeiites to olivine melilitites from South Eastern Australia utilizing geochemical and experimental petrological data. *J. Pet.*, 19, 463–513.
- Genik, G. J. (1993). Petroleum geology of cretaceous-tertiary rift basins in Niger, Chad, and Central African Republic. *Am. Assoc. Petrol. Geol. Bull.*, 77, 1405–1434.
- Gourgaud, A. and Vincent, P. M. (2003). Petrology of two continental alkaline intraplate series at Emi Koussi volcano, Tibesti, Chad. *J. Volc. Geotherm. Res.*, 129, 261–290.
- Green, D. H. (1973). Conditions of melting of basanite magma from garnet peridotite. *Earth Planet. Sci. Lett.*, 17(2), 456–465.
- Gsell, J. and Sonnet, J. (1962). *Prospection de reconnaissance sur la coupure de Niéré (feuille de Niéré N° ND 34 NE 0.80-E.8)*. Institut Equatorial de Recherches et d'Etudes Géologiques et Minières.
- Guiraud, R. and Maurin, J.-C. (1992). Early Cretaceous rifts of Western and Central Africa: an overview. *Tectonophysics*, 213, 153–168.
- Haggerty, S. E. and Tompkins, L. A. (1984). Subsolidus reactions in Kimberlitic ilmenites: exsolution, reduction and the redox state of the mantle. *Dev. Petrol.*, 6, 335–357.
- Halliday, A. N., Davidson, J. P., Holden, P., Dewolf, C., Lee, D.-C., and Fitton, J. G. (1990). Trace element fractionation in plumes and the origin of HIMU mantle beneath the Cameroon line. *Nature*, 347, 523–528.
- Halliday, A. N., Lee, D.-C., Tommasini, S., Davies,

- G. R., Paslick, C. G., Fitton, J. G., and James, D. E. (1995). Incompatible trace elements in OIB and MORB and source enrichment in the sub-oceanic mantle. *Earth Planet. Sci. Lett.*, 133, 379–395.
- Hofmann, A. W., Jochum, K. P., Seufert, M., and White, W. M. (1986). Nb and Pb in oceanic basalts: new constraints on mantle evolution. *Earth Planet. Sci. Lett.*, 79, 33–45.
- Irvine, T. N. and Baragar, W. R. A. (1971). A guide to the chemical classification of the common rocks. *Can. J. Earth Sci.*, 8, 523–548.
- Kagou Dongmo, A., Nkouathio, D. G., Pouclet, A., Bardintzeff, J.-M., Wandji, P., Nono, A., and Guillou, H. (2010). The discovery of late quaternary basalt on Mount Bambouto: implications for recent widespread volcanic activity in the southern Cameroon Line. *J. Afr. Earth Sci.*, 57, 96–108.
- Kagou Dongmo, A., Wandji, P., Pouclet, A., Vicat, J. P., Cheilletz, A., Nkouathio, D. G., Alexandrov, P., and Tchoua, F. M. (2001). Évolution volcanologique du mont Manengouba (Ligne du Cameroun); nouvelles données pétrographiques, géochimiques et géochronologiques. *C. R. Acad. Sci.*, 333, 155–162.
- Kamenetsky, V. M., Crawford, A. J., and Meffre, S. (2001). Factors controlling chemistry of magmatic spinel: an Empirical study of associated olivine, Cr-spinel and Melt Inclusions from primitive rocks. *J. Petrol.*, 42(4), 655–671.
- Kamgang, P., Chazot, G., Njonfang, E., and Tchoua, F. M. (2008). Geochemistry and geochronology of mafic rocks from Bamenda Mountains (Cameroon): Source composition and crustal contamination along the Cameroon volcanic line. *C. R. Geosci.*, 340, 850–857.
- Kamgang, P., Njonfang, E., Chazot, G., and Tchoua, F. (2007). Géochimie et géochronologie des laves felsiques des monts Bamenda (ligne volcanique du Cameroun). *C. R. Geosci.*, 339(10), 659–666.
- Kogbe, C. A. (1981). Cretaceous and tertiary of the Iullemeden basin in Nigeria (West Africa). *Cretac. Res.*, 2, 129–186.
- Le Bas, M. J., Le Maître, R. W., Streckeisen, A., and Zanettin, B. (1986). A chemical classification of volcanic rocks based on the total alkali-silica diagram. *J. Petrol.*, 27, 745–750.
- Louis, P. (1970). *Contribution géophysique à la connaissance géologique du bassin du lac Tchad*, volume 42 of *Bulletin de l'Office de la Recherche Scientifique et Technique Outre-Mer*. ORSTOM, Paris.
- Marzoli, A., Piccirillo, E. M., Renne, P. R., Bellieni, G., Iacumin, M., Nyobe, J. B., and Tongwa, A. T. (2000). The Cameroon volcanic line revisited: Petrogenesis of continental basaltic magmas from lithospheric and asthenospheric mantle sources. *J. Petrol.*, 41, 87–109.
- Marzoli, A., Renne, P. R., Piccirillo, E. M., Castorina, F., Bellieni, G., Melfi, A. G., Nyobe, J. B., and N'ni, J. (1999). Silicic magmas from the continental Cameroon volcanic line (Oku, Bambouto and Ngaoundere):  $^{40}\text{Ar}$ - $^{39}\text{Ar}$  dates, petrology, Sr-Nd-O isotopes and their petrogenetic significance. *Contrib. Mineral. Petrol.*, 135, 133–150.
- Mbassa, B. J., Njonfang, E., Benoit, M., Kamgang, P., Grégoire, M., Duchene, S., Brunet, P., Ateba, B., and Tchoua, F. M. (2012). Mineralogy, geochemistry and petrogenesis of the recent magmatic formations from Mbengwi, a continental sector of the Cameroon volcanic line (CVL), Central Africa. *Mineral. Petrol.*, 106, 217–242.
- Mbowou, G. I. B., Lagmet, C., Nomade, S., Ngounouno, I., Bernard Déruelle, B., and Ohnenstetter, D. (2012). Petrology of the late cretaceous peralkaline rhyolites (pantellerite and comendite) from Lake Chad, Central Africa. *J. Geosci.*, 57, 127–141.
- Mchargue, T. R., Heidrick, T. L., and Livingstone, J. (1992). Tectonostratigraphic development of the Interior Sudan Rifts, Central African. *Tectonophysics*, 213, 187–202. *Geodynamics of Rifting, Vol. II. Case History Studies on Rifts: North and South America and Africa.*
- Middlemost, E. A. K. (1975). The basalt clan. *Earth Sci. Rev.*, 11, 337–364.
- Milesi, J. P., Frizon de Lamotte, D., De Kock, G., and Toteu, F. (2010). In CGMW and UNESCO, editors, *Tectonic Map of Africa (2nd edited), scale 1: 10,000,000*. CCGM-CCGM, Paris.
- Morimoto, N., Fabriès, J., Ferguson, A. K., Ginzburg, I. V., Ross, M., Seifert, F. A., Zussman, J., Aoki, K., and Gottardi, G. (1988). Nomenclature of pyroxenes. *Am. Min.*, 73, 1123–1133.
- Ngounouno, I., Déruelle, B., and Demaiffe, D. (2000). Petrology of the bimodal Cenozoic volcanism of the Kapsiki plateau (northernmost Cameroon, Central Africa). *J. Volc. Geotherm. Res.*, 102, 21–44.
- Niu, Y. and O'Hara, M. J. (2003). Origin of ocean island basalts: A new perspective from petrology, geochemistry, and mineral physics considerations. *J. Geophys. Res. Solid Earth*, 108, article no. 2209.

- Nkouandou, O. F., Ngounouno, I., and Deruelle, B. (2010). Géochimie des laves basaltiques récentes des zones Nord et Est de Ngaoundéré (Cameroun, Plateau de l'Adamaoua, Afrique centrale): pétrogenèse et nature de la source. *Intern. J. Biol. Chem. Sci.*, 4(4), 984–1003.
- Nzenti, J. P., Barbey, P., Macaudière, J., and Soba, D. (1988). Origin and evolution of the late Precambrian high-grade Yaoundé gneisses (Cameroon). *Precambrian Res.*, 38, 91–109.
- Pearce, J. A. (1982). Trace element characteristics of lavas from destructive plate boundaries. In Thorpe, R. S., editor, *Andesites: Orogenic Andesites and Related Rocks*, pages 525–548. Wiley, Chichester.
- Pearce, J. A. (1983). The role of sub-continental lithosphere in magma genesis at destructive plate margins. In Hawkesworth, C. J. and Norry, M. J., editors, *Continental Basalts and Mantle Xenoliths*, pages 230–249. Shiva, Nantwich.
- Pilet, S., Baker, M. B., and Stolper, E. M. (2008). Metasomatized lithosphere and the origin of alkaline lavas. *Science*, 320, 916–919.
- Poudjom Djomani, Y. H., Diament, M., and Albouy, Y. (1992). Mechanical behaviour of the lithosphere beneath the Adamawa uplift (Cameroon, West Africa) based on gravity data. *J. Afr. Earth Sci.*, 15(1), 81–90.
- Poudjom Djomani, Y. H., Diament, M., and Wilson, M. (1997). Lithospheric structure across the Adamawa plateau (Cameroon) from gravity studies. *Tectonophysics*, 273, 317–327.
- Reusch, A., Nyblade, A., Wiens, D., Shore, P., Ateba, B., Tabod, C., and Nnange, J. (2010). Upper mantle structure beneath Cameroon from body wave tomography and the origin of the CVL. *Geochem. Geophys. Geosyst.*, 11, article no. Q10W07.
- Shellnutt, J. G., Lee, T. Y., Torng, P. K., Yang, C. C., and Lee, Y. H. (2016). Late Cretaceous intraplate silicic volcanic rocks from the Lake Chad region: An extension of the Cameroon volcanic line? *Geochem. Geophys. Geosyst.*, 17, 2803–2824.
- Sun, S. S. and McDonough, W. F. (1989). Chemical and isotopic systematic of oceanic basalts: implications of mantle composition and processes. In Saunders, A. . and Norry, M. ., editors, *Magmatism in Ocean Basins*, volume 42 of *Geological Society, London, Special Publications*, 42, pages 313–345. Geological Society of London.
- Tiabou, A. F., Temdjim, R., Wandji, P., et al. (2018). Baossi-Warack monogenetic volcanoes, Adamawa Plateau, Cameroon: petrography, mineralogy and geochemistry. *Acta Geochim.*, 38(1), 40–67.
- Tokam Kanga, A., Tabod Tabod, C., Nyblade, A. A., Juliá, J., Douglas, A. W., and Pasyanos, E. M. (2010). Structure of the crust beneath Cameroon, West Africa, from the joint inversion of Rayleigh wave group velocities and receiver functions. *Geophys. J. Int.*, 183, 1061–1076.
- Vicat, J. P., Pouclet, A., Bellion, Y., and Doumnang, J. C. (2002). Les rhyolites hyperalkalines (pantelérîtes) du lac Tchad. Composition et signification tectonomagmatique. *C. R. Geosci.*, 334, 885–891.
- Wandji, P., Bardintzeff, J. M., Ménard, J. J., and Tchoua, F. M. (2000). The alkaline fassaite bearing volcanic province of Noun plain (West-Cameroon). *N. Jahrb. Miner. Mh.*, 1, 1–14.
- Wang, N., Ostuni, E., Whitesides, G. M., and Ingber, D. E. (2002). Micropatterning tractional forces in living cells. *Cell Motil. Cytosk.*, 52, 97–106.
- Weaver, B. L. (1991). The origin of ocean island basalt end-member compositions: trace element and isotopic constraints. *Earth Planet. Sci. Lett.*, 104, 38–397.
- Wyllie, P. J. (1977). Mantle fluid compositions buffered by carbonates in peridotite CO<sub>2</sub>-H<sub>2</sub>O. *J. Geol.*, 85, 187–207.
- Xu, C., Huang, Z., Qi, L., Fu, P., Liu, C., Li, E., and Gung, T. (2007). Geochemistry of Cretaceous granites from Mianning in the Panix region, Sichuan Province, southwestern China: implications for their generation. *J. Asian. Earth Sci.*, 29, 737–750.
- Ye, J., Chardon, D., Rouby, D., Guillocheau, F., Dalasta, M., Ferry, J.-N., and Broucke, O. (2017). Paleogeographic and structural evolution of northwestern Africa and its Atlantic margins since the early Mesozoic. *Geosphere*, 13(4), 1254–1284.
- Yokoyama, T., Aka, F. T., Kusakabe, M., and Nakamura, E. (2007). Plume-lithosphere interaction beneath Mt. Cameroon volcano, West Africa: Constraints from <sup>238</sup>U-<sup>230</sup>Th-<sup>226</sup>Ra and Sr-Nd-Pb isotope systematic. *Geochim. Cosmochim. Acta*, 71, 1835–1854.
- Zindler, A. and Hart, S. R. (1986). Chemical geodynamics. *Annu. Rev. Earth Planet. Sci.*, 721(14), 493–571.